Article

Not peer-reviewed version

Effect of Annealing Conditions of High-Energy Ball-Milled Sm(Fe, CO, Ti)12 Alloys Doped with Zr on Microstructure and Magnetic Properties

Margarit Gjoka *, Charalampos Sarafidis, Dimitrios Niarchos, George Hadjipanayis

Posted Date: 26 February 2025

doi: 10.20944/preprints202502.2139.v1

Keywords: Rare earth permanent magnets; high energy ball-milling; magnetic properties; crystal structure

Article

Effect of Annealing Conditions of High-Energy Ball-Milled Sm(Fe, Co, Ti)$_{12}$ Alloys Doped with Zr on Microstructure and Magnetic Properties

Margarit Gjoka [1,*], Charalampos Sarafidis [2], Dimitrios Niarchos [1] and George Hadjipanayis [3,4]

[1] Institute of Nanoscience and Nanotechnology, National Centre for Science and Research "Demokritos," 15341 Athens, Greece

[2] Department of and Physics, School of Sciences, Aristotle University of Thessaloniki, 54124 Thessaloniki, Greece

[3] Department of Physics, University of Delaware, Newark, DE 19713, USA

[4] Department of Chemical Engineering, Northeastern University, Boston, MA 02115, USA

* Correspondence: m.gjokas@inn.demokritos.gr

Abstract: The tetragonal $R_{1-x}Zr_x$ $(FeCo)_{11}Ti$ alloys, where R is a rare earth and Ti is a transition metal, are promising candidates for permanent magnets. $Sm_{1-x}Zr_x(Fe_{0.8}Co_{0.2})_{12-y}Ti_y$ (x=0 and 0.25; y=1 and 0.7) master alloys were prepared by arc-melting under argon atmosphere. Two samples with equal atomic amount of Ti are almost single-phase compounds 1:12 with a small amount of a-Fe(Co), while after replacing Sm with Zr a small amount of the $Sm(FeCo)_2$ Laves phase appeared in the other two samples. The as-cast ingots were milled using high-energy ball milling (HEBM) for different times in an argon atmosphere then annealed at 973K-1173K at different interval times (15-90 min. After annealing, the sample milled for 4 h contains a large variation of grain size from 2-4 μ to 20 μ or larger. While the others sample milled for 8 h, after annealing exhibits grains size in the range of 2-6 μ, therefore their coercivity is higher, reaching a maximum value of 5.5 kOe for $SmFe_9Co_2Ti$ annealed at 1123K for 60 min. Coercivity was strongly affected by the annealing temperature and time. The microstructure evolution with emphasis on the particles size during annealing and their correlation with coercivity will be discussed.

Keywords: rare earth permanent magnets; high energy ball-milling; magnetic properties; crystal structure

1. Introduction

The challenging, world-wide environmental problems are the main driving factor of a series of important technological advances. Sustainable transportation and effective electricity production like offshore wind generators have skyrocketed the demand for materials suitable for permanent magnets (PM). Extensive demand induces challenges in production and supply channels making necessary the development of new materials, especially with low content in critical raw metals like the rare earths (RE) or other important ones like Co [1–5].

The tetragonal $ThMn_{12}$-type alloys with nominal composition $R(Fe,T)_{12}$, where R is a rare-earth atom and T is a transition metal atom, are excellent candidates for permanent magnets due to their high Curie temperature, large magnetization, and strong uniaxial magneto-crystalline anisotropy, as well as of low RE content compared to other magnetic alloys. Magnetization and intrinsic anisotropy outperform well established magnetic materials and Curie temperatures are high enough even close to 600 K, establishing a working temperature higher than that of $Nd_2Fe_{14}B$ without the need of doping with heavy RE atoms [6–8]. Coercivity values above 10 kOe (μ_0H 1 T) have been observed [9] and the fact that all these properties are combined with the largest T/RE ratio in the relevant families of compounds explains why these alloys are on the focus of scientific research in recent years [10,11].

$SmFe_{12}$ binary alloy is thermodynamically unstable but the addition of a transition element T (T = Ti, Mo, V, Al, Si, Ga) may assist in stabilizing the tetragonal structure for the $RFe_{12-x}T_x$ series, with Ti being the most favored element. However, these additions result in a decline of the magnetic

 doi:10.20944/preprints202502.2139.v1

properties [12–19]. This has led to investigations for achieving minimal use of Ti in $SmFe_{12}$ based compounds as those reported in [16,20]. Another prominent path is by replacing Fe with Co, it is well known that this specific substitution affects both stability and the magnetic properties of the RE-T intermetallics so it has the potential to stabilize the tetragonal 1:12 phase. The 3d magnetocrystalline anisotropy constant remains uniaxial for relatively small Co replacement for Fe and room temperature K1 reaches about 0.9 MJm^{-3} [19]; with up to 20% Co replacement for Fe anisotropy does not affect anisotropy field significantly while at the same time the magnetization is improved. The maximum magnetization of the -non-existing in bulk- theoretical compound $SmFe_{12}$ could be as high as 160 Am^2/kg [20]. In an early survey of $SmTiFe_{11-x}Co_x$ alloys reported by S. F. Cheng et al. [21] it was found that the tetragonal phase could be stabilized for $x \leq 2$ while maintaining the easy magnetization direction along the c-axes. This is important since it is very often in these systems that Co favors a different type of magnetocrystalline anisotropy. For replacement beyond $x = 2$, other phases such as 2:17 usually appear while the magnetic moments are canted in a conical arrangement [21]. Hirayama et al. have reported that $ThMn_{12}$ type structure can also be stabilized by Co addition in epitaxially grown thin films with nominal composition $Sm(Fe_{0.8}Co_{0.2})_{12}$ [22]. Furthermore, they found that the intrinsic hard magnetic properties were superior even to those of $Nd_2Fe_{14}B$ with a Curie temperature of (859 K), an anisotropy field of 1.2 T, and a spontaneous magnetization of 1.78 T. There are also many reports on $Sm(FeT)_{12}$ (T= Ti, Mo, V, Al, Si, Ga) alloys and their ribbons produced by melt-spinning or strip flakes, as well as the their isotropic powders that were produced by rapid solidification or mechanical alloying [9,11,13–15,23–26]. Because of their low remanent magnetization, these isotropic powders need more improvements in processing in order to be used as a basis for PM applications. There are also reports on nanocomposite powders for $Sm(FeCoT)_{12}$ alloys. Additionally the effect of particle size on the thermal decomposition of powders with nominal composition $Sm(Fe_{0.8}Co_{0.2})_{11}Ti$, $Sm(Fe_{0.8}Co_{0.2})_{10}VTi$, $Sm(Fe_{0.8}Co_{0.2})_{10.5}Ga_{0.5}Ti$ and $Sm(Fe_{0.8}Co_{0.2})_{10.5}Cu_{0.5}Ti$, which were prepared by jet-mill and then were annealed is reported as well as the case of annealed $Sm_8Fe_{73.5}Ti_8V_8Ga_{0.5}Al_2$ alloy. The latter was pulverized using the nitrogen jet-milling process, obtaining particles with an average size of 2-5 μm, and then the sintering process was followed. The importance of the type and the concentration of the additional stabilizing T elements is also outlined [26,27].

It was observed a very interesting result after substitution of Sm by Zr, which can improve the magnetic properties under certain conditions. Zr is known for its ability to substitute for both RE or T atoms in similar compounds, in these $ThMn_{12}$-based tetragonal alloys the partial substitution of Sm for Zr stabilizes the structure of $Sm(FeCo)_{12}$ alloys [20]; surprisingly the saturation magnetization increases further for the case of $Sm_{0.74}Zr_{0.26}(Fe_{0.8}Co_{0.2})_{12}$ compound reaching a value of $\mu_0Ms = 1.9$ T [20,28,29], which is the largest saturation magnetization ever achieved in such intermetallic alloys. Yao et al. measured lower magnetization close to $\mu_0Ms = 1.4$ T but with very high anisotropy constants ($K_1 = 3.04$ MJm^{-3}, $K_2 = 0.57$ MJm^{-3}) and increased Curie temperature close to 675 K in ribbons of nominal composition $Sm_{0.74}Zr_{0.26}(Fe_{0.8}Co_{0.2})_{12}$ [31].

This path was further exploited in literature, rapidly quenched materials produced by either by the melt spinning technique with nominal stoichiometry $(SmR)(FeCo)_{12-x}Ti_x$ (R=Y, Zr) or the strip-casting method of $(R,Zr)(Fe,Co)_{12-x}Ti_x$ (R = Nd and Sm) alloys [30–33] were also used to produce materials with interesting magnetic properties. The advancement of computational tools has also led to relevant contributions where Zr was also found to positively affect magnetization as in other, previously reported cases [28,34–36]. Additionally, the thermodynamic stability of the Fe rich compounds can be improved using the multi-element alloying approach, which can also minimize the degradation of magnetic properties [20,33,37,38].

Following the specific improvement path, a few years ago we had presented preliminary results of high-energy ball milled (HEBM) of $Sm_{1-x}Zr_x(Fe_{0.8}Co_{0.2})_{12-y}Ti_y$ (x=0 and 0.25; y=1 and 0.7) materials [39]. Partial substitution of Sm with Zr significantly improves the properties of these compounds and their potential for applications as PM [11]. While Ti is very effective element to thermodynamically stabilize the tetragonal structure, it has the drawback that it degrades the magnetic properties [12]. Introduction of Zr may assist in stabilizing the structure while reducing Ti content [31]. Kobayashi et

 doi:10.20944/preprints202502.2139.v1

al. explained this stabilizing effect by examining the average Fe-Fe interatomic distances at Fe(8i), Fe(8j), and Fe(8f) sites. They have observed that the iron atoms in 8i positions are arranged in a distance very large than their atomic radii; larger Ti atoms may provide a way to accommodate the parge interatomic distance and make the metallic hybridization possible. Incorporation of Zr, which is smaller than Sm, may assist in that direction [33].

It is evident that the specific system has large potential. In the present study we extend the previous work by providing a wider view of HEBM powders of Sm(Fe, Co, Ti)$_{12}$ alloys doped with Zr, focusing on the effect of annealing conditions of powders on microstructure and magnetic properties.

2. Materials and Methods

$Sm_{1-x}Zr_x(FeCo)_{12-y}Ti_y$ (, x=0 and 0.25; y=1 and 0.7) alloys were prepared by arc-melting in a high purity argon atmosphere and with excess Sm content to compensate for evaporation during melting. The nominal composition of the first two series of alloys were $SmFe_9Co_2Ti$ (A-series) and $SmFe_{9.04}Co_{2.26}Ti_{0.7}$ (B-series) respectively. For the other two alloys we have partially substituted Zr for Sm and the nominal composition was $Sm_{0.75}Zr_{0.25}Fe_9Co_2Ti$ (C-series) and $Sm_{0.75}Zr_{0.25}Fe_{9.04}Co_{2.26}Ti_{0.7}$ (D-series). Parts from all sample series were mechanically treated in a high energy ball milling device (HEBM) for different milling times (4 and 8 hours) in argon atmosphere in order to produce an amorphous or partially disordered phase. The weight ratio of balls to powder was 10:1. A combination of balls with diameter 12, 8, 5.5 and 4 mm was used. All samples were subsequently annealed at different times (15-90 min) and temperatures (973K-1173K) in order to recrystallize the 1:12 phase and achieve improved coercivity.

X-ray diffraction (XRD) data of powder samples were obtained using a SIEMENS D500 diffractometer with Cu–Kα radiation in the range 2θ =20-90 degrees 2θ and step 0.03°/5 s. The magnetic properties of the alloys were determined by thermomagnetic analysis (TMA) and a Vibrating Sample Magnetometer (VSM). Thermomagnetic analysis data was obtained under an external field of about 0.015 T (μ_0H) using small pieces. Magnetization measurements were also performed at room temperature on magnetically oriented powders fixed in epoxy resin under an applied field up to 3 T (μ_0H). XRD measurements on magnetically aligned powders were also carried out to study the magnetocrystalline anisotropy of the materials. Particle sizes and their distribution was estimated using Scanning Electron Microscopy (SEM).

3. Results and Discutions

3.1. Structure of Arc-Melting Alloys

According to the Rietveld analysis, two of the as-cast samples with atomic content of Ti equal to 1 (samples A and C) were almost single-phase with the with tetragonal 1:12 $ThMn_{12}$-type structure (No 139, Space Group *I4/mmm*) where Ti and Co atoms were assumed to be arranged at 8*i* and 8*f*-sites, respectively. In Figure 1 the corresponding X-ray diffraction plot is presented for the sample A. The unit cell parameters **a** and **c** for 1:12 phases are 0.8557 and 0.4784 nm respectively. Impurity α-

 doi:10.20944/preprints202502.2139.v1

(Fe,Co) phase appeared with minor content, maximum 1.24 wt.% and a unit cell parameter a = 0.2885 nm, slightly larger than the corresponding value of α-Fe.

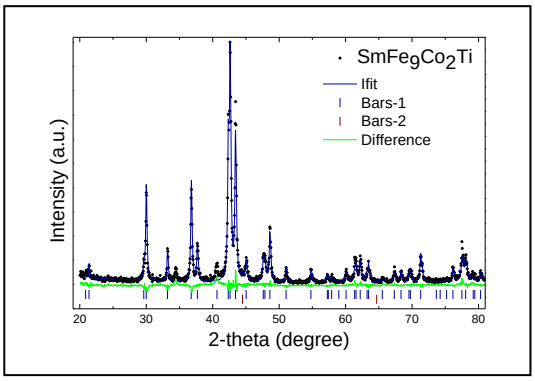

Figure 1. XRD spectrum of arc melted $SmFe_9Co_2Ti$ alloy refined by Rietveld method. : (▪) are experimental points. The continuous line corresponds to the calculated spectrum. Vertical bars (I) and (II) at the bottom indicate the position of the Bragg peaks for 1:12 phase and α-(FeCo) respectively. The continuous line at the bottom is the difference between the experimental intensity values and the calculated one.

In Figure 2 the thermomagnetic curves of all as casted alloys are presented. The curves of the samples A and C exhibit two magnetic transitions at 739(5) and 1216(5) K, for the 1:12 and α-(FeCo) phases respectively. The apparent high magnetic transition of α-(FeCo) is affected from the 1:12 phase. The curie transitions of α-(FeCo), depending on the amount of both Fe and Co, are usually in the range 1193-1258K [32].

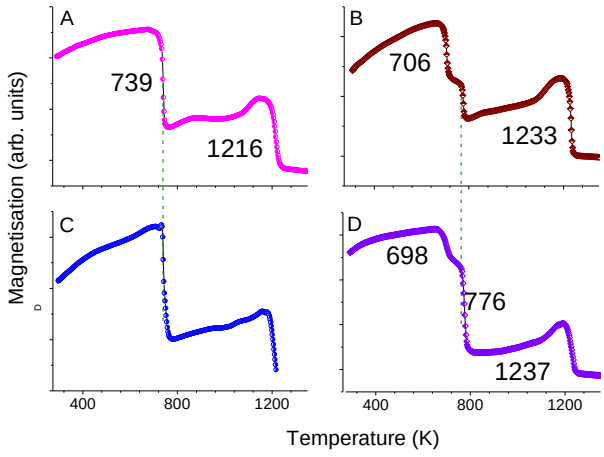

Figure 2. Thermomagnetic curves of as-cast alloys, $SmFe_9Co_2Ti$ (A), $Sm\ Fe_{9.04}Co_{2.26}Ti_{0.7}$ (C), $Sm_{0.75}Zr_{0.25}Fe_9Co_2Ti$ (C) and $Sm_{0.75}Zr_{0.25}Fe_{9.04}Co_{2.26}Ti_{0.7}$ (D).

When Sm was partially substituted by Zr, a third phase $Sm(FeCo)_2$ of $ZnMg_2$ Laves-type appears (samples C and D) for both cases independently of Ti content, either Ti content equals 1 or 0.7. The Curie temperatures of these additional phases are 706(5) and 698 (5) K for the samples C and D respectively. It's worth mentioning that the Curie temperature for $SmFe_2$ compound is 700 K [41]. The Curie temperature for the 1:12 phase is 776 K for both samples B and D, close to that reported before in the literature [20,21,33,36]. Zr has a negative effect on the Curie temperature, but the increase of Co amount compensates, and the compound retains a relatively large temperature endurance, for the case of sample D. The magnetic transitions of the minor α-(FeCo) phase were detected at 1233(5) and 1237(5) K for the samples C and D respectively (Figure 2), probably related to minor deviations of the Co content in α-(FeCo) minority phase.

 doi:10.20944/preprints202502.2139.v1

Structure and Magnetic Properties of High-Energy Ball Milling (HEBM)

The as-cast ingots were milled using high-energy ball milling (HEBM) for different milling times; 4 and 8 hours in Ar atmosphere, maintaining a mass ratio of balls to powder 10:1. All samples after milling exhibit an amorphous/disordered phase, as it was shown in the Figure 3a for $SmFe_9Co_2Ti$. Only a broad reflection appears at the area of 44 degrees 2θ, which belongs to the α-(FeCo) partially crystallized into larger grains.

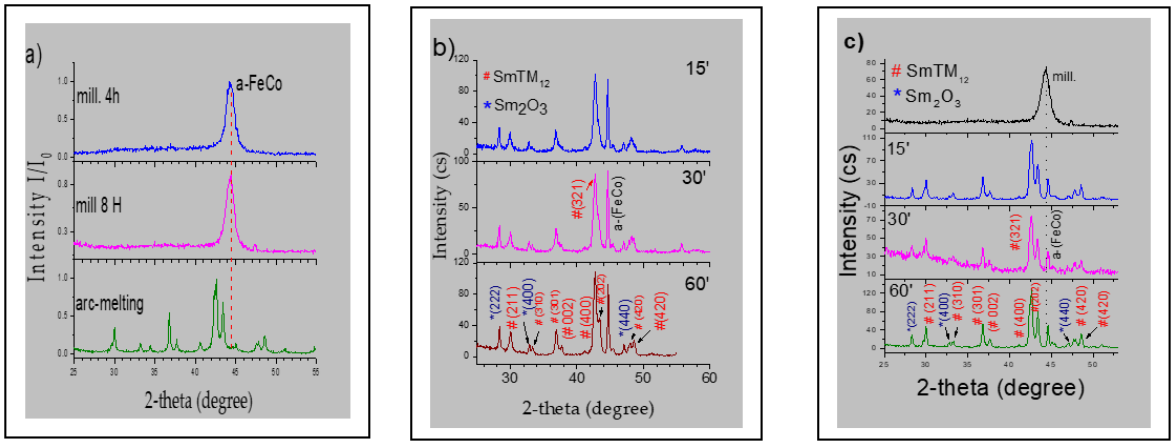

Figure 3. a) XRD of $SmFe_9Co_2Ti$ powders milled for 4 h and 8h respectively; **b)** XRD diagrams of annealed powder of $SmFe_9Co_2Ti$ milled for 4 h at 1073K 15, 30 and 60 minutes and the respective Miler's indexes of 1:12 and Sm_2O_3 **c)** XRD diagrams of annealed powder of $SmFe_9Co_2Ti$ milled for 4 h at 1123K 15, 30 and 60 minutes.

After thermal treatment at temperatures ranging from 973 to 1173K for different periods of time (15-90 min), the amorphous powders recrystallized in a 1:12 majority phase, however with slightly larger α-(FeCo) content. A small amount of Sm_2O_3 oxided is formed, thethe respective Milers index are shown in the Figure 3b. The possibility of the appearance of other phases like $Sm(FeCo)_2$ with $MgZn_2$ structure and 2:17 could not be excluded due to the similarity in the relevant XRD patterns, however they respective reflections are barely seen . Typical X-ray diffraction pattern for sample A milled for 4 h and annealed at the range 15-60 min are presented in Figure 3b.

SEM images show that the grain sizes of the samples depend strongly on the annealing time and as a profound consequence the coercivity also depends on the annealing time. The powder of sample A milled for 4 h after annealing contains a large variation of grain size from 2-4 μ to 20 μ or larger, and such wide range of grain sizes is not optimal for increasing the coercivity, as was evident from SEM images. Sample A milled for 8 h exhibits grain sizes mainly in the range of 2-6 μ after annealing; this is a rather optimum annealing time in this case (Figure 4).

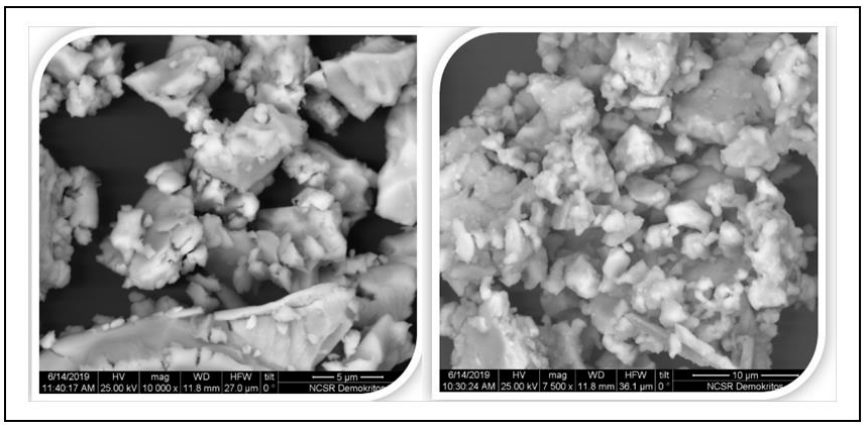

Figure 4. SEM images of anneled powder of $SmFe_9Co_2Ti$ at 1123 K milled for 4h (on the left) and 8 h(on the right).

Preprints.org (www.preprints.org) | NOT PEER-REVIEWED | Posted: 26 February 2025 doi:10.20944/preprints202502.2139.v1

In Figure 5 the demagnetization curves of sample A milled for 4 h and annealed at different intervals of time (15-90 minutes) and temperature range 973 K-1173 K are presented. The coercivity reaches the maximum value of 4.6 kOe (0.46 T $\mu_0 H_C$) for the sample annealed at 1073 K for 60 minutes, while the magnetization decreases from 123 Am^2/kg for the sample annealed during 15 minutes to 118 Am^2/kg for annealing for 60 minutes. The $SmFe_9Co_2Ti$ samples annealed at 1173 K exhibit a higher amount of a-(Fe,Co) than when annealed at 1073 K, and this can explain their moderate coercivity values, which reaches a maximum of 4.04 kOe (0.40 T $\mu_0 H_C$) after annealing for 30 min.

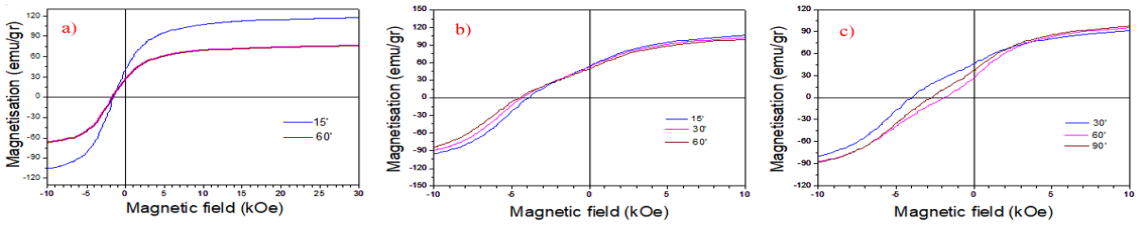

Figure 5. Demagnetization curves of annealed $SmFe_9Co_2Ti$ powders at 973 K (a), 1073 K (b) and 1173 K (c), all samples were milled during 4 h.

Figure 6a presents the demagnetization curves of sample A annealed at 1123 K, measured up to a maximum field of $\mu_0 H$ = 3 T. The specific mass magnetization at the maximum external field decreases slightly from 115 Am^2/kg (annealing 15 minutes) to 105 Am^2/kg (annealing time 60 minutes). The trend of magnetization for the sample A at 973 K, 1073 K and 1173 K (milling time 4 h) and at 1123 K (milling time 8 h) is depicted in Figure 6b. The magnetization acquires values in the range between 105-123 Am^2/kg.

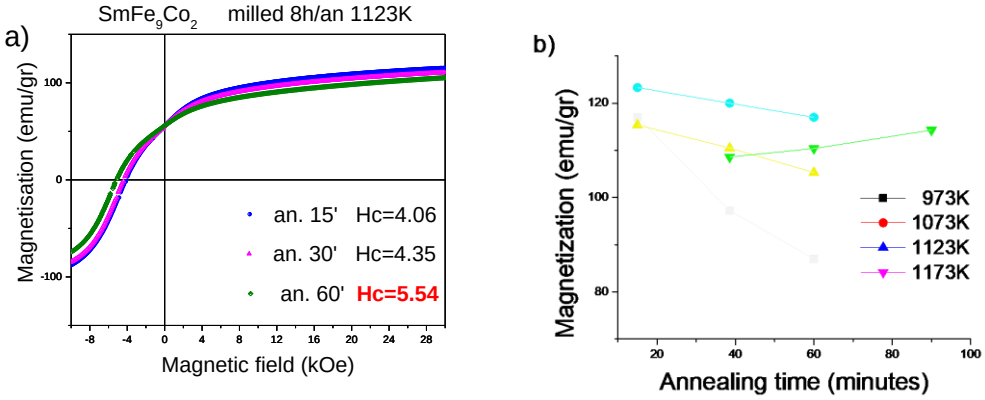

Figure 6. a) Demagnetization curves of annealed $SmFe_9Co_2Ti$ powders at 1123; **b)** the respective magnetization values at 3T of sample annealed at 973 K, 1073 K and 1173K (milled 4 h), and at 1123 K (milled 8 h).

The coercivity of Sample A reaches the highest maximum value of 5.5 kOe (0.55 T $\mu_0 H_C$) after annealing for 60 min, Figure 7a. However, this value was lower than it would be expected due to the precipitation of the soft α-(FeCo) phases, as it is evident in the X-ray diffraction plots (Figure 3b). Figure 7b shows the coercivity values of sample A milled for 4 and 8 hours and annealed at 1073 K and 1123 K, respectively, which suggests that the optimal annealing conditions to achieve the highest coercivity in our case is a temperature of 1123 K for 8 hours.

 doi:10.20944/preprints202502.2139.v1

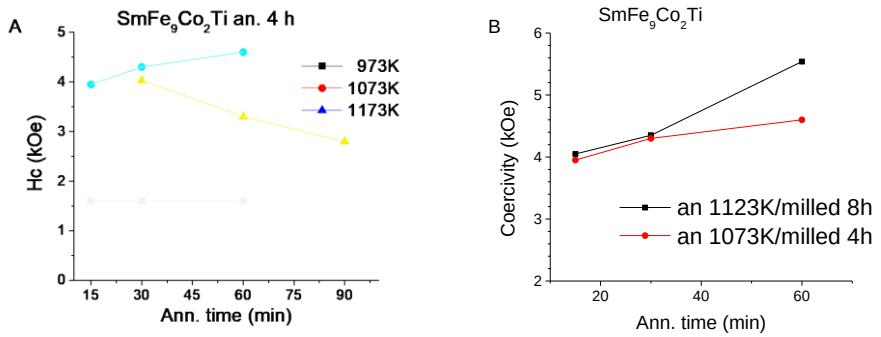

Figure 7. a) Coercivity values of $SmFe_9Co_2Ti$ powders annealed at 1123 K versus annealing time; **b)** optimal condition for maximum coercivity of sample A.

The demagnetization curves for the samples B, C and D annealed at 1098 K and 1123 K are shown in the Figure 8. The coercivity is below 4 kOe (0.40 T $\mu_0 H_C$) for samples C and D where Sm was partially substituted by Zr, however it improves to 4.3 kOe ((0.46 T $\mu_0 H_C$) after annealing at 1123 K for 60 minutes. The expected decreases of magnetization after Zr substitution at samples D is compensated by the decrease of Ti content. In the Table 1 are show the respective value of coercivity and magnetization, the value of magnetization are measured at 3 T, which is almost close to the saturation magnetization.

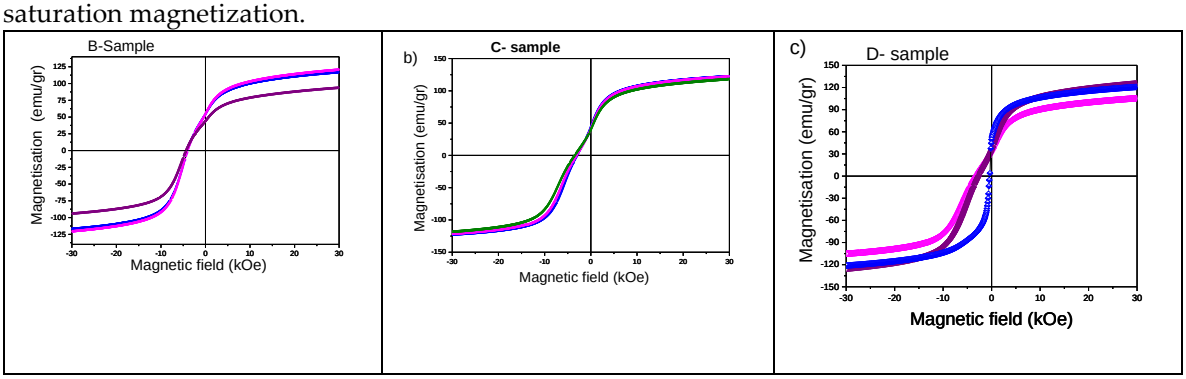

Figure 8. a) Demagnetization curves of sample B- $SmFe_{9.04}Co_{2.26}Ti_{0.7}$ annealed at 1123 K, **b)** Demagnetization curves of sample C-$Sm_{0.75}Zr_{0.25}Fe_9Co_2Ti$ annealed at 1098 K and **c)** sample D-$Sm_{0.75}Zr_{0.25}Fe_{9.04}Co_{2.26}Ti_{0.7}$ annealed at 1123 K.

Table 1. Coercivity and magnetization value of of sample B, C and D.

	Sample B ann. at 1123 K		**Sample C ann. at 1098 K**		**Sample D ann. at 1123 K**	
Ann. time	**Hc (kOe)**	**M_{3T} (emu/gr)**	**Hc (kOe)**	**M_{3T} (emu/gr)**	**Hc**	**M_{3T} (emu/gr)**
15 m	4.01	120.9	3.0	122.8	4.05	120.8
30 min	4.05	120.7	3.1	122.1	3.29	105.5
60 min	4.37	93.6	3.5	118.4	2.76	125.6

4. Conclusions

$SmFe_{12}$-based alloys, stabilized by Ti and Zr were prepared by arc-melting under argon atmosphere, aiming to investigate the magnetic properties of their annealed HEBM powders. The arc-melting samples without Zr were almost single-phase 1:12 compounds with a small amount of a-Fe(Co), while after substitution of Sm with Zr, a small quantity of $Sm(FeCo)_2$ Laves phase appeared. After milling, the samples exhibit an amorphous/disordered phase which was successfully recrystallized into a majority 1:12 phase after annealing. The milling time as well as the annealing process affects heavily the coercivity. The grain sizes of the samples milled for 8 h had a narrow distribution of 2 - 6 μm after annealing, while the grain sizes of the samples milled for 4 h had a wider distribution from 2 - 6 to 20 μm. As a result, the coercivity, as an external property related to the grain

 doi:10.20944/preprints202502.2139.v1

sizes, was higher for the annealed samples preliminarily milled for 8 h. A coercivity of $\mu_0 Hc = 0.55$ T was obtained for the sample A milled 8 h and annealed at 1123 K. However, there are still large grains smaller than 2 μm and larger than >6 μm for the applied experimental conditions, which would explain the moderate coercivity of the annealed samples. The coercivity decreased after substitution of Sm for Zr due to precipitation a third Laves phases and possible traces of other phases. The small amount of Sm-oxide affect negatively the coercivity.

Author Contributions: Conceptualization, methodology, validation, all authors; resources, D. N. and G. H.; data curation, M. G., C. S.; writing—original draft preparation, M. G.; writing—review and editing, M. G., C. S.; visualization, funding, supervision, M. G., D. N. and G. H. All authors have read and agreed to the published version of the manuscript.

Funding: This research was partially supported by H2020-NMP23-2015 NOVAMAG: Novel Materials by Design for substituting Critical Raw Materials.

Institutional Review Board Statement: Not applicable.

Informed Consent Statement: Not applicable.

Data Availability Statement: Available on request.

Conflicts of Interest. The authors declare no conflict of interest.

References

1. Popa D. C., Szabó L. Securing Rare Earth Permanent Magnet Needs for Sustainable Energy Initiatives, Materials **2024**, 17, 5442. https://doi.org/10.3390/ma17225442.
2. A European Green Deal. Available online: https://ec.europa.eu/info/strategy/priorities-2019-2024/european-green-deal_en (accessed on February 22nd, 2024).
3. Podmiljšak B., Saje B., Jenuš P., Tomše T., Kobe S., Žužek K., Šturm S., The Future of Permanent-Magnet-Based Electric Motors: How Will Rare Earths Affect Electrification? Materials **2024**, 17, 848. https://doi.org/10.3390/ma17040848
4. Filippas A., Sempros G., Sarafidis C., Critical rare earths: The future of Nd & Dy and prospects of end-of-life product recycling, Materials Today: Proceedings **2021**, 37, 4058–4063. https://doi.org/10.1016/j.matpr.2020.09.210
5. Wang X., Yao M., Li J., Zhang K., Zhu H. Zheng M., China's Rare Earths Production Forecasting and Sustainable Development Policy Implications, Sustainability **2017**, 9, 1003. https://doi.org/10.3390/su9061003
6. Mooij, D.B. De, and K.H.J. Buschow. Some Novel Ternary $ThMn_{12}$-Type Compounds. Journal of the Less Common Metals **1988**, 136(2), 207–215.
7. Hong-Shuo Li, and Coey J.M.D. Chapter 1 Magnetic Properties of Ternary Rare-Earth Transition-Metal Compounds. In Handbook of Magnetic Materials, Editor Buschow K.H.J. Publisher North Holland**;** 1991, Volume 6, pp 1-83.
8. Ohashi, K., Y. Tawara, R. Osugi, and M. Shimao. Magnetic Properties of Fe-rich Rare-earth Intermetallic Compounds with a $ThMn_{12}$ Structure. J. Appl. Phys. **1988**. 64 (10), 5714–16. https://doi.org/10.1063/1.342235.
9. Wang, Y.Z., and G.C. Hadjipanayis. Magnetic Properties of Sm-Fe-Ti-V Alloys. J. Magn. Magn. Mater. **1990**, 87 (3), 375–78. https://doi.org/10.1016/0304-8853(90)90774-K.
10. Wei J., Xu S., Xu C., Liu X., Pan Y., Wang W., Wu Y., Chen P., Liu J, Zhao L, Zhang X. Tuning Fe_2Ti Distribution to Enhance Extrinsic Magnetic Properties of $SmFe_{12}$-Based Magnets, Crystals **2024**, 14, 572. https://doi.org/10.3390/cryst14060572
11. Gabay, A.M., and G.C. Hadjipanayis. Mechanochemical Synthesis of Magnetically Hard Anisotropic $RFe_{10}Si_2$ Powders with Representing Combinations of Sm, Ce and Zr. J. Magn. Magn. Mater.**2017,** 422, 43–48. https://doi.org/10.1016/j.jmmm.2016.08.064.
12. Saengdeejing, A., Chen, Y. Improving Thermodynamic Stability of $SmFe_{12}$-Type Permanent Magnets from High Entropy Effect. *J. Phase Equilib. Diffus.* **2021**, 42, 592–605. https://doi.org/10.1007/s11669-021-00894-w.

13. Okada, M., K. Yamagishi, and M. Homma. High Coercivity in Melt-Spun $SmFe_{10}(TiV)_2$ Ribbons. Materials Transactions, JIM **1989,** 30 (5), 374–77. https://doi.org/10.2320/matertrans1989.30.374.
14. Okada, M., A. Kojima, K. Yamagishi, and M. Homma. High Coercivity in Melt-Spun SmFe10(Ti,M)2 Ribbons (M=V/Cr/Mn/Mo). IEEE Trans. Magn. **1990**, 26 (5), 1376–78. https://doi.org/10.1109/20.104383.
15. Wang, Y., Hadjipanayis G. C., Kim A., Liu N. C., and Sellmyer D. J. Magnetic and Structural Studies in Sm-Fe-Ti Magnets." J. Appl. Phys. **1990**, 67 (9), 4954–56. https://doi.org/10.1063/1.344745.
16. Tozman, P., H. Sepehri-Amin, T. Ohkubo, and K. Hono. Intrinsic Magnetic Properties of (Sm,Gd)Fe_{12}-Based Compounds with Minimized Addition of Ti. J. Alloy Compd. **2021**, 855, 157491. https://doi.org/10.1016/j.jallcom.2020.157491.
17. Hu, Bo-Ping, Hong-Shuo Li, J P Gavigan, and J M D Coey. Intrinsic Magnetic Properties of the Iron-Rich $ThMn_{12}$-Structure Alloys R($Fe_{11}Ti$); R=Y, Nd, Sm, Gd, Tb, Dy, Ho, Er, Tm and Lu. J. Phys. Condens. Matter **1989**, 1(4), 755–70. https://doi.org/10.1088/0953-8984/1/4/009.
18. R. Coehoorn. Electronic structure and magnetism of transition-metal-stabilized $YFe_{12-x}M_x$ intermetallic compound. Phys. Rev. B, **1990**, 41, 11790–11797. https://doi.org/10.1103/PhysRevB.41.11790.
19. Buschow, K.H.J. Permanent Magnet Materials Based on Tetragonal Rare Earth Compounds of the Type $RFe_{12-x}M_x$. J. Magn. Magn. Mater. **1991**, 100 (1–3), 79–89. https://doi.org/10.1016/0304-8853(91)90813-P.
20. Tozman, P., H. Sepehri-Amin, Y.K. Takahashi, S. Hirosawa, and K. Hono. Intrinsic Magnetic Properties of Sm(FeCo)$_{11}$Ti and Zr-Substituted $Sm_{1-y}Zr$ $(Fe_{0.8}Co_{0.2})_{11.5}Ti_{0.5}$ Compounds with $ThMn_{12}$ Structure toward the Development of Permanent Magnets." Acta Materialia **2018,** 153, 354–63. https://doi.org/10.1016/j.actamat.2018.05.008.
21. Cheng, S.F., V.K. Sinha, Y. Xu, J.M. Elbicki, E.B. Boltich, W.E. Wallace, S.G. Sankar, and D.E. Laughlin. Magnetic and Structural Properties of $SmTiFe_{11-x}Co_x$ Alloys. J. Magn. Magn. Mater. **1988**, 75 (3), 330–38. https://doi.org/10.1016/0304-8853(88)90039-X.
22. Hirayama, Y., Y.K. Takahashi, S. Hirosawa, and K. Hono. Intrinsic Hard Magnetic Properties of $Sm(Fe_{1-x}Co_x)_{12}$ Compound with the $ThMn_{12}$ Structure. Scr. Mater. **2017**, 138, 62–65. https://doi.org/10.1016/j.scriptamat.2017.05.029.
23. L. Schultz, K. Schnitzke, J. Wecker. High coercivity in mechanically alloyed Sm-Fe-V magnets with a $ThMn_{12}$ crystal structure, Appl. Phys. Lett. **1990**, 56, 868–870. https://doi.org/10.1063/1.102662.
24. Zhang, J. S., Tang, X., Sepehri-Amin, H., Srinithi, A. K., Ohkubo, T., & Hono, K. Origin of coercivity in an anisotropic Sm(Fe,Ti,V)$_{12}$-based sintered magnet. Acta Materialia, **2021**, 217, 117161. https://doi.org/10.1016/j.actamat.2021.117161
25. Zhou T.H., Zhang B., Zheng X., Song Y., Si P., Choi C.J., Cho Y.R., Park J., Anisotropic $SmFe_{10}V_2$ Bulk Magnets with Enhanced Coercivity via Ball Milling Process, Nanomaterials **2024**, 14, 1329. https://doi.org/10.3390/nano14161329
26. Xu C., Wen L., Pan A., Zhao L., Liu Y., Liao X., Pan Y., Zhang X., First-Principles Study of Ti-Doping Effects on Hard Magnetic Properties of $RFe_{11}Ti$ Magnets, Crystals **2024**, 14, 507. https://doi.org/10.3390/cryst14060507
27. Dirba, I., H. Sepehri-Amin, Ik-Jin Choi, Jin-Hyeok Choi, Hyoun-Soo Uh, Tae-Hoon Kim, Soon-Jae Kwon, T. Ohkubo, and K. Hono. SmFe12-Based Hard Magnetic Alloys Prepared by Reduction-Diffusion Process. J. Alloy Compd. **2021**, 861, 157993. https://doi.org/10.1016/j.jallcom.2020.157993.
28. Tozman, P., Y.K. Takahashi, H. Sepehri-Amin, D. Ogawa, S. Hirosawa, and K. Hono. The Effect of Zr Substitution on Saturation Magnetization in $(Sm_{1-x}Zr_x)(Fe_{0.8}Co_{0.2})_{12}$ Compound with the $ThMn_{12}$ Structure." Acta Materialia **2019**, 178, 114–21. https://doi.org/10.1016/j.actamat.2019.08.003.
29. Tozman, P., H. Sepehri-Amin, and K. Hono. Prospects for the Development of $SmFe_{12}$-Based Permanent Magnets with a $ThMn_{12}$-Type Phase. Scr. Mater. **2021**, 194, 113686. https://doi.org/10.1016/j.scriptamat.2020.113686.
30. Lim, Jung Tae, Hui-Dong Qian, Jihoon Park, Chul-Jin Choi, and Chul Sung Kim. Crystal Structure and Magnetic Properties of Fe-Rich $Sm(Fe_{0.8}Co_{0.2})_{11}Ti$ Permanent Magnetic Materials. Journal of the Korean Physical Society **2019**, 74 (12): 1146–50. https://doi.org/10.3938/jkps.74.1146.

31. Yao, Y.F., Hou Y.H., Li H.F., Chai W.X., Wu Z.J., Feng Q., Li W., Pang Z.S., Ma L., Yu H.B., Huang Y.L., Microstructure and Magnetic Properties of Exchange-Coupled Nanocomposite $Sm_{0.75}Zr_{0.25}(Fe_{0.8}Co_{0.2})_{11}Ti$ Alloy. J. Magn. Magn. Mater. **2023**, 571, 170578. https://doi.org/10.1016/j.jmmm.2023.170578.
32. Hagiwara M., Sanada N., and Shinya Sakurada. Structural and Magnetic Properties of Rapidly Quenched $(Sm,R)(Fe,Co)_{11.4}Ti_{0.6}$ (R = Y, Zr) with $ThMn_{12}$ Structure." AIP Adv. **2019**, 9, 035036. https://doi.org/10.1063/1.5079949.
33. Kobayashi, K., Suzuki S., Kuno T., Urushibata K., Sakuma N., Yano M., Shouji T., Kato A., Manabe A.. The Stability of Newly Developed (R,Zr)(Fe,Co)12−xTix Alloys for Permanent Magnets. J. Alloy Compd. **2017**, 694, 914–20. https://doi.org/10.1016/j.jallcom.2016.09.311.
34. Liu, F., Feng H., Zhao H., Xu S., Magnetic Properties and Microstructure of Ce and Zr Synergetic Stabilizing Ti-Lean $SmFe_{12}$-Based Strip-Casting Flakes. J. Magn. Magn. Mater. 2024, **599**, 172100. https://doi.org/10.1016/j.jmmm.2024.172100.
35. Matsumoto, M., Hawai T., Ono K, $(Sm,Zr)_xFe_{12-x}M_x$ (*M*=Zr,Ti,Co) for Permanent-Magnet Applications: Ab Initio Material Design Integrated with Experimental Characterization. Phys. Rev. App. **2020**, 13 (6), 064028. https://doi.org/10.1103/PhysRevApplied.13.064028.
36. Landa A., Söderlind P., Moore E., Perron A., Thermodynamics and Magnetism of $SmFe_{12}$ Compound Doped with Zr, Ce, Co and Ni: An Ab Initio Study, Metals **2024**, 14, 59. https://doi.org/10.3390/met14010059
37. Martin-Cid, A., Salazar, D., Schönhöbel, A. M., Garitaonandia, J. S., Barandiaran, J. M., & Hadjipanayis, G. C. Magnetic properties and phase stability of tetragonal $Ce_{1-x}Sm_xFe_9Co_2Ti$ 1:12 phase for permanent magnets. Journal of Alloys and Compounds, **2018**, 749, 640–644. https://doi.org/10.1016/j.jallcom.2018.03.325
38. Li Y., Yu N., Wu Q., Pan M., Zhang S., Ge H., Role and optimization of thermal annealing in $Sm_{0.74}Zr_{0.26}(Fe_{0.8}Co_{0.2})_{11}Ti$ alloys with $ThMn_{12}$ structure. J. Magn. Magn. Mater., **2022**, 549, 169065. https://doi.org/10.1016/j.jmmm.2022.169065.
39. Gjoka M., Sarafidis C., Niarchos D. and Hadjipanayis G.C. Evolution of microstructure and magnetic properties in annealed high energy ball milled $Sm(Fe, Co, Ti)_{12}$ compounds doped, with Zr. In *Proceedings of the* 64th of Annual Conference on Magnetism and Magnetic Materials, 4-8 November Las Vegas 2019, Abstract Book p. 603
40. R. S. Sundar& S. C. Deevi. Soft magnetic FeCo alloys: alloy development, processing, and properties, International Materials Reviews 2005, 50(3), 157-192, https://doi.org/10.1179/174328005X14339
41. Christodoulou C. N., Takeshita T. Hydrogenation and nitrogenation of $SmFe_2$, Journal of Alloys and Compounds, 1993, 194(1), 31-40. https://doi.org/10.1016/0925-8388(93)90641-Y.